Engineering Fracture Mechanics 269 (2022) 108525

Contents lists available at ScienceDirect

Engineering Fracture Mechanics

journal homepage: www.elsevier.com/locate/engfracmech

# Squat initiation mechanism model in a rail-wheel contact

Sandra Baltic *, Werner Daves

*Materials Center Leoben Forschung GmbH, Roseggerstraße 12, A-8700 Leoben, Austria*

ARTICLE INFO

*Keywords:*
Squat
Rail damage
Rolling contact fatigue
Configurational force
Finite element analysis

ABSTRACT

Observations in a railway track frequently show the start of a squat-form crack right next to the wheel-rail running band on the rail head surface. This article investigates the potential of a head check-like surface defect near the running band to initiate a squat formation. Cross sectioning of the rail samples having squats in the initial stage of development suggested the crack initiation in a transverse plane (perpendicular to the rail traffic direction), implying that broadening to a typical squat shape in the longitudinal direction (rail traffic direction) occurs afterwards. The influence of possible factors that might trigger the squat formation particularly on the transverse plane across the rail is elaborated in the numerical study. The tendency of one defect to grow rather than another is analysed by configurational force theory in order to determine both the crack driving force value and the crack growth direction. The effect of the contact patch variations and changed frictional properties at the crack faces on the squat-like crack development are studied in detail. The numerical results show that analysed cracks are able to grow under particular wheel loading in the directions that are in accordance with observed squat growth. These results suggest lateral forces as one of the main suspected determinants favouring the squat initiation.

## 1. State-of-the-art

Squat-type rail cracks are characterised by a localised depression of the rail-wheel running band and specific lobby-shape [36,46]. A squat-type crack typically starts on a rail head surface and grows to a depth of a few millimetres [28]. Upon broadening in the rail traffic direction, referred to as the longitudinal direction in the continuation, the subsurface crack grows parallel to the rail head surface. In its mature stage of development, the crack can either turn up and end by a spallation of some rail pieces or turn down in the rail profile, leading to a catastrophic failure. Although the railway rails are designed to endure consecutive heavy loading on a long-term basis, squat-type cracks often call for premature replacements of rail segments to ensure reliability and safety of the rail traffic.

Squat-form cracks tend to appear both in harder and softer rail steel grades, in curved and straight tracks, in high-speed and conventional routes, on the railway lines with passenger, freight or mixed traffic. For instance, the contributions of [10], [18] and [35] report on the experiences of Japanese, Australian and British railway networks, respectively. This tenacious occurrence of squats has given rise to worldwide research efforts to understand the initiation mechanism behind.

The review works [23,44,45] witness the substantial work and progress made in the research on squats and their origination theories. While some studies in the literature place more emphasis on a particular track feature, e.g. foundation [19] or welds [33], others focus on the dynamic rail-wheel interaction, e.g. [26], among others. The most recent literature [35] implies that rail grinding

* Corresponding author at: Roseggerstraße 12, A-8700 Leoben, Austria.
*E-mail address:* sandra.baltic@mcl.at (S. Baltic).

https://doi.org/10.1016/j.engfracmech.2022.108525
Received 10 February 2022; Received in revised form 27 April 2022; Accepted 2 May 2022
Available online 6 May 2022

plays an essential role in controlling the development of squats. This hypothesis is in accordance with the work of Rasmussen et al. [38] who argued that the side effects of the grinding process substantially favour the initiation of rolling contact fatigue (RCF) cracks in a rail steel. In particular, it was shown that the cracks tend to initiate in the areas of spatial material property gradients, i.e. at the martensite/pearlite interface.

It becomes apparent that there are many different aspects of the theory proposing plausible explanations for squat initiation, however, none of them has been worked out to such an extent that the squats would be reproducible under controlled laboratory conditions, i.e. on a test rig. This underscores the need for additional model-based assessments to benchmark numerous potential causal factors (and their combinations) and single out only the essential ones.

In this work, an attempt is made to identify the main parameters governing the squat initiation from a mechanical point of view. A sample having squat-type cracks in the initial stage of development is extracted from a rail in service. Particular emphasis is put on the crack broadening transversally and longitudinally across and along the rail profile. Looking closely at the squat cracks in the rail sample, it could be assumed that the crack started to grow first in the direction perpendicular to the rail traffic direction, that is, in a

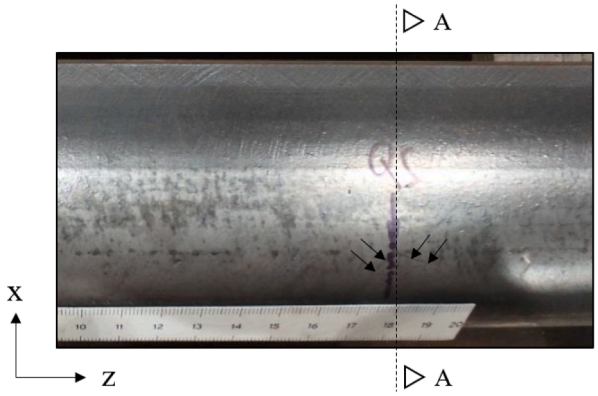


(a)

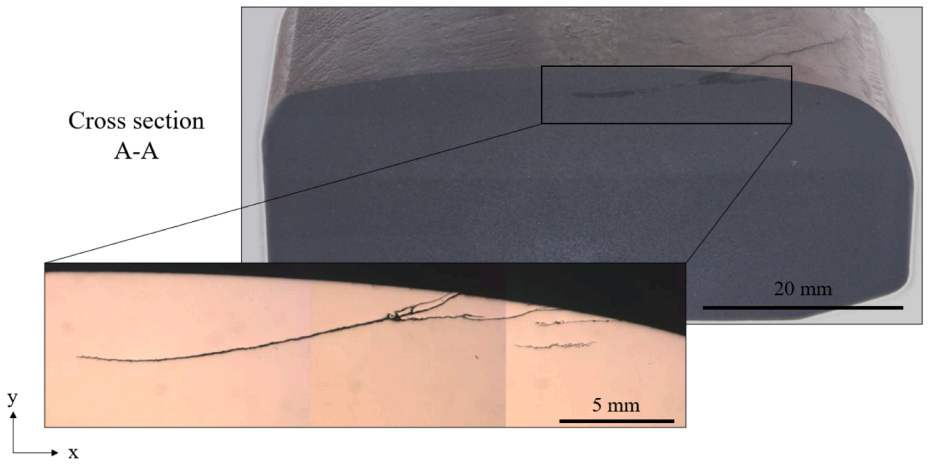


(b)

**Fig. 1.** Rail sample with the surface squat in the initial stage: (a) top view, (b) transversal cross section.

transverse plane. Therefore, the squat initiation stage on a transverse plane section across the rail requires a special attention.

A computational model of a rail cross section is built up and a pre-crack just like the observed real pre-crack geometry is introduced in the model. Using the configurational force theory [13,30,31], the crack driving forces and their directions are determined at the pre-crack tip. The numerical model allows to assess the potential crack growth across different loading events, altered pre-crack positions and changed frictional properties at the crack faces. For particular case studies, calculated crack growth directions are found to be in accordance with squat-type crack propagation directions recorded by metallographic microscopy. These cases suggest the lateral forces as one of the main suspected determinants favouring the squat-type crack initiation from a mechanical point of view.

## 2. Squat-type crack initiation: Visual inspection

For the investigation of the critical conditions that cause the squat initiation, a representative example of a squat form crack in the initial stage of development has been analysed. Fig. 1a shows a rail sample having a mild squat on the rail surface. The arrows on the Fig. 1a point to the V-shaped crack visible on the rail head surface. The rail sample has been taken from a curved track of a radius 1480 m. The rail track was a part of a mixed railway traffic system experiencing a load of approximately 60 000 tons per day.

The rail sample has been cut in transversal direction to the rail traffic (Fig. 1b) at the position where a squat type crack is visible. From the metallographic examination in Fig. 1b it is evident that after reaching the depth of 5 mm the crack tends to grow in the direction almost parallel to the running surface. This is the main characteristic of squat type cracks which grow parallel to the surface and either turn up, spalling smaller pieces of the rail, or turn down in the rail leading to derailment.

Furthermore, when closely looking at the metallographic investigation in Fig. 1b, one can conclude that a squat-like crack can initiate from head checks with the initial crack angle between 20° and 30°. Squat crack initiates near the running band on the rail head, as frequently reported in the literature, [43,28,25], among others. First in more advanced stages of development squats show typical visual characteristics like a localised depression of the rail surface having the shape of a lobe or a lung. Thus, for the squat initiation stage, the crack growth mechanisms on a transverse plane seem to play an important role. Therefore, herein we restrict ourselves to the crack analysis in the transversal direction only, as illustrated in Fig. 2.

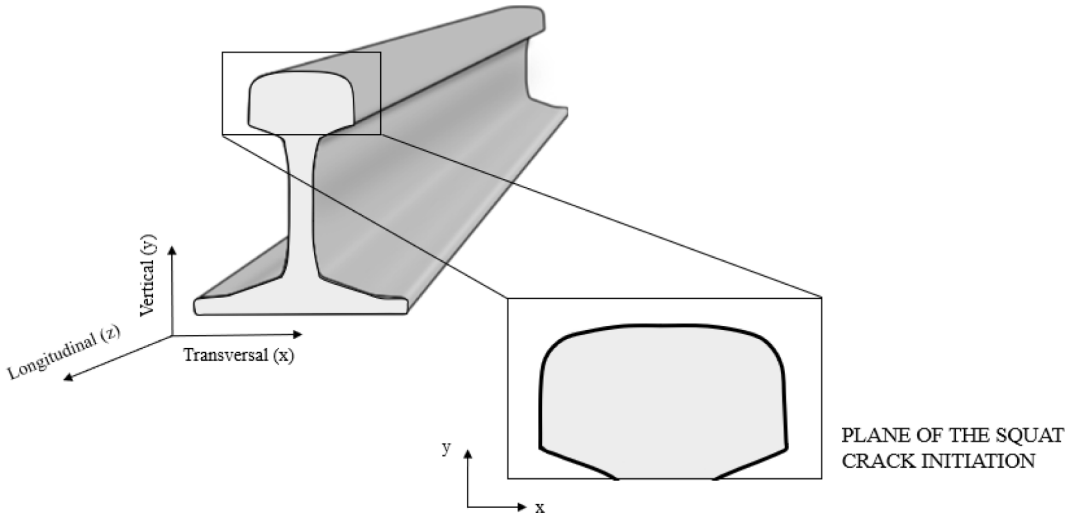


**Fig. 2.** Terminology used for the directions in a rail. Plane of the squat type crack initiation (XY plane) is considered in the numerical studies.

## 3. Computational models

### 3.1. Finite element model

The pearlitic rail steel sample is considered as a homogeneous solid and modelled using elasticity theory. The computational model consists of two parts, namely a rail and a wheel profile cross section, see Fig. 3. In this way, it is possible to model a more realistic wheel-rail contact interaction. Since merely the rail head region is of interest for squat initiation mechanism, the rail web and foot are disregarded in the model.

The contact pair consists of a new 60E1 (UIC60) rail profile and a new S1002 wheel geometry. The model is built up in the ANSYS Mechanical simulation software. 4-node plane strain elements (PLANE182 element type of the ANSYS element library [2] with unit thickness are used to discretize the complete model. The mesh of the finite element model is designed such that the elements in the rail-wheel contact region feature the same element size. Thus, the respective region is discretized by a uniform mesh of 0.4 mm element size. Approaching the upper wheel's and lower rail's boundary, the element size is slightly coarsened to 1 mm to save the number of elements in the model.

ANSYS contact elements are used to model the contact between two deformable surfaces i.e. rail and wheel boundaries. The rail and wheel contact surfaces are overlaid by CONTA172 and TARGE169 contact elements, respectively, thereby defining a contact pair in the model. After meshing the model parts independently, the rail-wheel contact pair is joined by making use of ANSYS internal algorithm for establishing the initial contact between the contact boundaries. The Lagrange multiplier contact formulation is used for modelling the rail-wheel contact. A dry contact is assumed between the rail and wheel surface and therefore the friction coefficient of 0.5 is adopted.

Nodal degrees of freedom (DOFs) at the rail's lower boundary are constrained in X and Y directions, as it is shown in Fig. 4. Furthermore, the nodal DOFs along the wheel's upper boundary are coupled and their motion is controlled by a reference node, see Fig. 4. The reference node is used to apply concentrated vertical and transversal nodal forces representing the wheel loading. The vertical wheel dead load is varied in the range of 5 to 15 kN in order to investigate the effect of maximum contact pressure on the potential crack growth. Furthermore, to examine the influence of the transversal forces occurring in a rail-wheel contact either because of eccentric vertical loading of wheels or hunting of passenger vehicles, the transversal load is varied between 0 and 3 kN.

Looking closely at the transversal cross section of the analysed rail sample (Fig. 1b), one can observe that the crack first appeared at the rail surface and grew in-plane. Therefore, the crack is assumed to have initiated at the rail surface and a surface defect having a length of 1 mm has been introduced in the rail head model accordingly. Such a crack can be seen as a head check or even as a residual crack after grinding stemming from a former head check. The finite elements along the defect geometry are detached to represent a pre-crack originating at the rail surface, see Fig. 3. The size of the finite elements along the predefined crack is 0.1 mm, which corresponds to 1/10 of the crack length. For modelling the contact interaction between the crack faces, the Lagrange multiplier contact

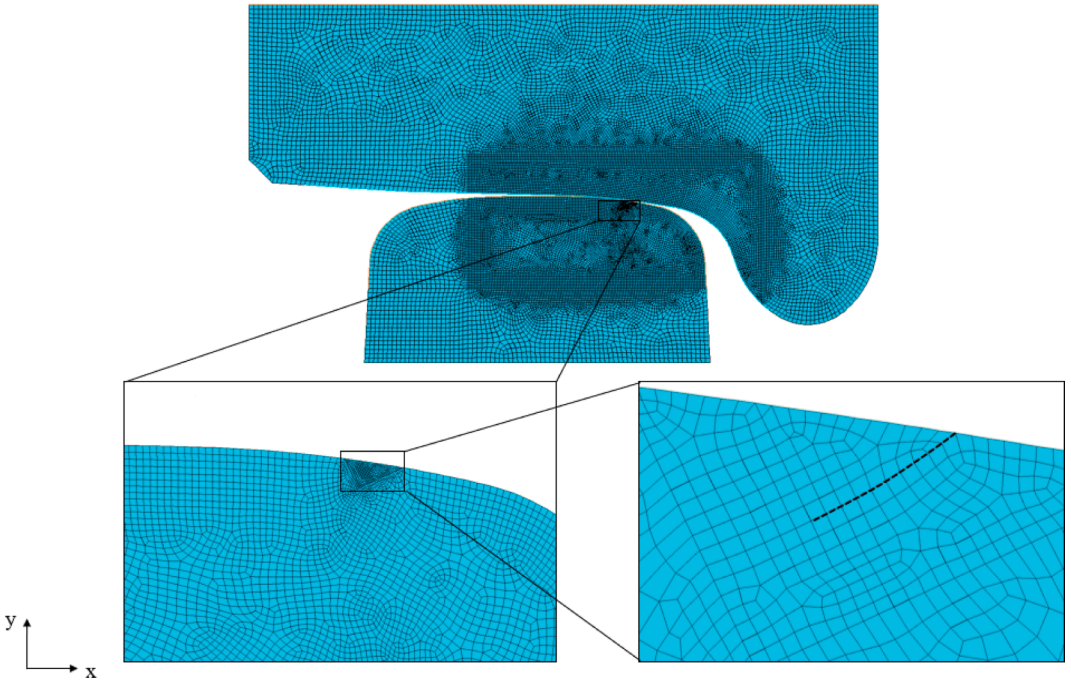


**Fig. 3.** Two-dimensional finite element model of the wheel-rail contact interaction. The finite elements along the marked (dashed) line are separated to model a surface defect.

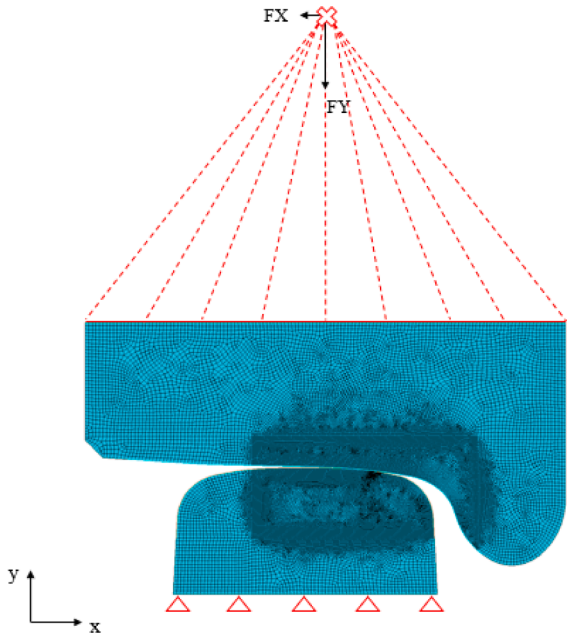


**Fig. 4.** Boundary conditions of the finite element model: the nodes at the wheel's top boundary are coupled to the marked reference node. The vertical and horizontal forces are imposed in the reference node. The nodes of the rail's lower boundary are fixed in X and Y direction.

formulation is used to avoid crack face interpenetration and the friction coefficient of 0.5 is initially assumed.

### 3.2. Calculation of the crack driving force

The configurational force concept [30] is used to calculate the crack driving forces in an elastically deformed rail material at the instant of a wheel passing a rail. The analysed rail has a surface defect i.e. a pre-crack in the immediate vicinity of the contact patch. Although the crack driving forces in an elastically deformed material could also be determined by contour path J-integralRice [39], the configurational force concept provides an additional essential information about the preferred crack propagation direction. Knowing the crack growth angle allows to contrast the simulation predictions with observed squat-type crack growth and thereby assess the possibility of a crack growth following the specific squat-type crack pattern.

Configurational or material forces are thermodynamic driving forces acting on the defects found in the material [16–17]. These defects can be e.g. dislocations or cracks. The configurational forces as vectoral quantities point in the preferred direction of a defect movement, that is, in the direction in which the total energy of the system is minimal. Based on the Eshelby's energy momentum tensor [16–17], the configurational force concept allows to derive the J-integral for incremental elastic–plastic material description Simha et al. [41], Simha et al. [42].

Generally speaking, in a 2D finite element model, the nodal configurational forces are evaluated as

$$f = \sum_{e=1}^{n} \int_{\beta} (-\nabla N \bullet \Sigma) d\beta, \tag{1}$$

where $\Sigma$ denotes the Eshelby stress tensor and $\nabla N$ is the matrix containing the gradients of the shape functions corresponding to a specific node. To calculate the total configurational force at one node, e.g. at the crack tip node, it is necessary to collect the configurational forces from $n$ finite elements surrounding the respective node in the integration domain $\beta$.

The Eshelby stress tensor in the finite strain elasticity yields to.

$$\Sigma_{ij} = w\delta_{ij} - F_{ij}P_{ij} \tag{2}$$

In the Eq. (2), $w$ denotes the strain energy density, $F_{ij}$ is the deformation gradient computed from the element shape functions, $P_{ij}$ is the first Piola-Kirchoff stress tensor and $\delta_{ij}$ stands for Kronecker delta.

By introducing the nodal unit vector $e$ in the crack growth direction, the energy dissipated per unit crack extension can be determined as.

$$F = e \bullet (-f) \tag{3}$$

Following the works of [29,30], the crack growth direction in a homogeneous and isotropic material can be determined using a thermodynamics-based maximum energy dissipation criterion. The dissipation $\psi$ at the crack tip that moves with a velocity $v$ is thus.

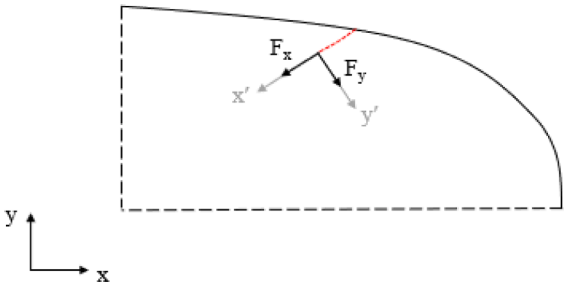


**Fig. 5.** The local coordinate system at the crack tip: x represents the tangential component with respect to the crack surface, y corresponds to the normal component of the local coordinate system. $F_x$ and $F_y$ are the components of the crack driving force for mode I and II, respectively.

$$\psi = (-f) \bullet v \rightarrow max \tag{4}$$

After decomposing $F$ into two perpendicular directions in a local coordinate system at the crack tip (see Fig. 5), the crack growth direction $\varphi$ can be calculated:

$$\varphi = arctan\left(\frac{F_y}{F_x}\right) \tag{5}$$

where $F_x$ and $F_y$ are the crack driving force components oriented in the direction of x and y axis of the local coordinate system, respectively. In the following sections the crack propagation direction is therefore determined using Eq. (5). For an in-depth discussion of fracture mechanics approach to determining the direction of crack extension review works can be consulted (Kolednik 2012, Özenc 2013). The magnitude of the crack driving force is calculated as.

$$F_M = \sqrt{F_x{}^2 + F_Y{}^2}. \tag{6}$$

## 4. Results and discussion

The actual rail profile geometry, which is frequently altered by maintenance activities, plays a decisive role in a rail-wheel contact interaction. The smaller contact area, the higher pressure develops within the contact patch. To investigate how this affects the crack growth, finite element analyses are performed for a range of contact patches that might occur in service. In particular, the contact patches having the maximum pressure in the range of 1000–2000 MPa are considered, as shown in Fig. 6. Different maxima are achieved by varying the normal load. This in turn leads to the change in broadness of the contact patch, as shown in Fig. 6. Specifically,

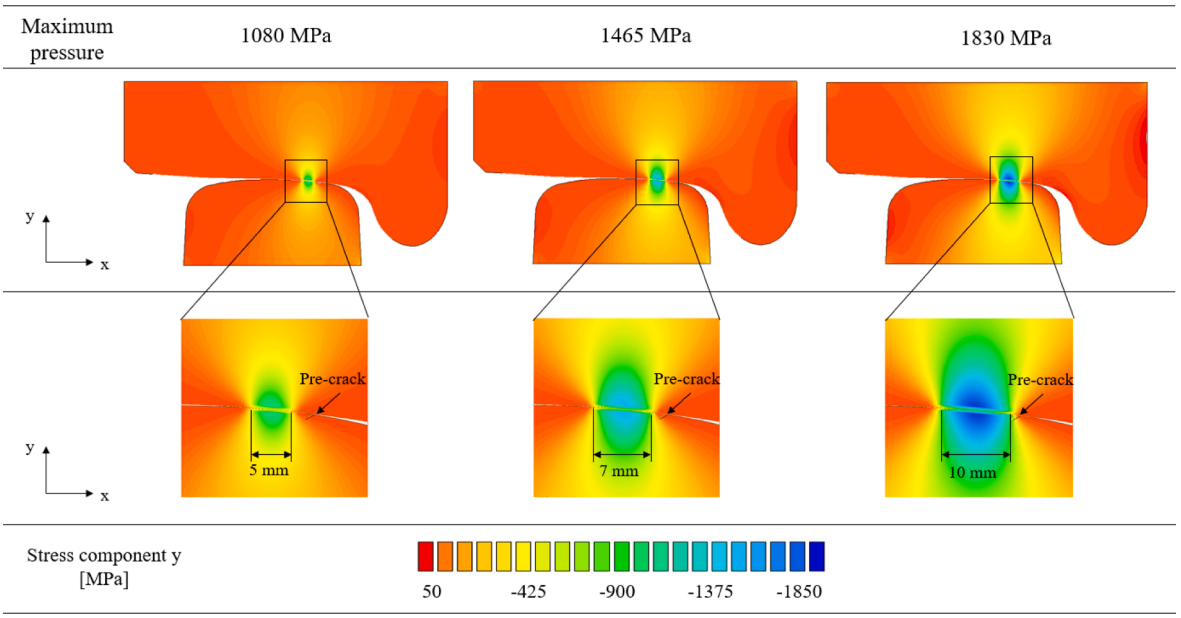


**Fig. 6.** Visualisation of the calculated stress distribution in y direction for three different levels of normal load (5, 10 and 15 kN). The enlarged views show broadening of the contact patch with increasing maximum pressure.

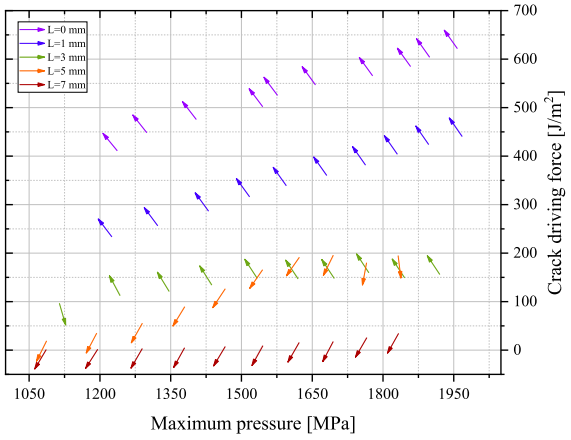


**Fig. 7.** Numerically computed crack driving forces at the crack tip with respect to the maximum pressure in the contact patch. The origin of each arrow indicates the calculated force magnitude. The arrows show the direction of the calculated crack growth direction. The crack initial position L relative to the centre of the contact patch is varied between 0 and 7 mm.

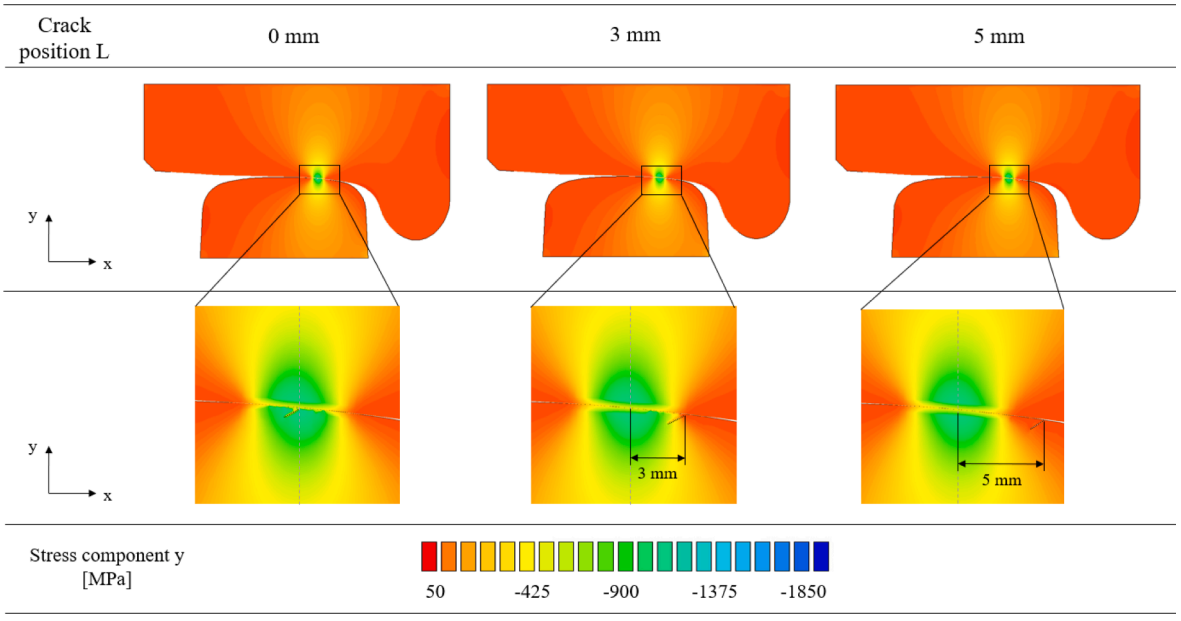


**Fig. 8.** Visualisation of the numerically computed stress distribution in y direction for the contact patch with maximum pressure of 1080 MPa and three different initial crack positions L. Enlarged views show the distance L measured from the centre of the contact patch.

the resulting contact patch size ranges from 5 to 10 mm. Below, all the numerical results for analysed contact patches will be presented in terms of calculated crack driving forces and their directions. The crack driving forces are evaluated for the first integration contour.

For numerical investigation of the impact of the contact patch on the squat-like crack development, altering the crack initial position is selected instead of any lateral displacing of the wheel and maintaining the crack position constant. This is because altering the wheel position in the model is very likely to alter the contact point between rail and wheel, leading to possibly more complex contact patch forms (e.g. 2-point-contact). This would make any analysis of a single mechanical aspect independently of other interrelations impossible.

Fig. 7 shows numerically predicted crack driving forces depending on the maximum pressure for altered crack initial positions denoted by L. For instance, in the case of $L = 0$ the start of the crack at the surface is placed in the centre of the contact patch (see Fig. 8). On the other hand, $L = 5$ is assigned to the initial crack position shifted by 5 mm from the contact patch's centre (see Fig. 8). In Fig. 7, the origin of a single arrow corresponds to determined crack driving force magnitude while the arrow points to the calculated crack propagation direction.

Provided that a threshold crack driving force value of 150 J/m$^2$ is sufficient for the crack initiation in a rail steel, likewise in [32], a threshold stress intensity factor of 5.9 MPa $\sqrt{m}$ can be calculated from the relation of the crack driving force to the stress intensity

factor [13]. Published experimental works also frequently report that the crack propagation threshold value ranges as low as 4 to 8 MPa $\sqrt{m}$ (70 to 280 J/m$^2$) in steel grades having a pearlitic microstructure, e.g. [15] or more recently IN2TRACK Project Report - Research into enhanced tracks, switches and structures [24]. Ideally, a fatigue crack growth kinetics for mixed mode would be available as only the combination of opening and shear modes can explain the crack paths observed in rails. However, it is still a great challenge to get an insight into pure mode II with current experimental mechanics. Nevertheless, these experimental limitations have gained great scientific interest and are thus the subject of ongoing research ([9], [40], among others).

Furthermore, it has long been recognized that there is a correlation of the equivalent crack growth threshold stress intensity factor to the elastic modulus for different materials [47], [48]. Wasén and Heier [47] suggested that the crack growth threshold stress intensity factor is directly proportional to the elastic modulus for a wide range of metallic materials. Specifically for steel the relation gives a threshold stress intensity factor of about 3–4 MPa $\sqrt{m}$.

For the reasons discussed above, the computed crack driving forces reaching the threshold value of 150 J/m2 are considered sufficient for crack growth. From the results shown in Fig. 7 it becomes apparent that particularly for the cracks placed inside the contact patch (L = 0, L = 1 and L = 3 mm) the crack driving forces attained high values ($\geq$200 J/m$^2$) sufficient for the crack growth. However, the corresponding crack growth directions indicate turning up which would lead to spalling some pieces of the rail rather than a squat-like crack growth. On the contrary, the cracks positioned right next to or even away from the contact patch (L = 5, L = 7) boundary prefer to propagate downward inside the rail head. This is a feature of the squat-type cracks turning down and causing the fracture of the rail. Yet the computed crack driving forces for the respective crack locations out of the contact patch zone (L = 5, L = 7) is evidently too low to cause the crack growth. In probing the problem further, other possible parameters that may favour the squat growth will thus be examined. In the continuation we restrict ourselves to the analysis of the cracks positioned right next to or away from the contact patch, since the study cases considered herein with contact patch on the crack appear to be relevant for rail defects other than squats.

Besides, it is worth noting that for case study with initial crack location L = 5 mm the crack driving force increases with increasing the maximum pressure (see Fig. 7). Recall that the respective crack is located next to the contact patch. The crack driving forces for the case study with L = 7 mm, in contrast, remain stable across various contact patches i.e. they are independent of the maximum pressure. Note that for a single crack location L the predicted crack growth direction appears to be uniform across different levels of the maximum pressure.

Though other RCF cracks can turn down in the rail as well, in the context of this work, downward crack propagation can be regarded as a benchmark for potential risk of a squat crack initiation. In this way, various potential causal factors, which are many, can at least be narrowed down.

The results of the finite element simulations which, in addition, consider transversal forces in a rail-wheel contact are shown in Fig. 9. In real track situations, higher transversal forces may appear due to e.g. yaw angles of the wheel caused by curves, hunting of vehicles etc. The transversal force in the negative direction of the x-axis (see Fig. 4) is varied between 0 and 3 kN, which corresponds to 20% of normal load in the extreme case. Fig. 9a shows numerically calculated crack driving forces at the crack tip for the initial position L = 5 mm. Recall that for this study case the crack is placed right next to the contact patch. Provided that the maximum pressure is between 1000 and 1300 MPa, a higher portion of transversal force can foster the crack propagation downward inside the rail. Furthermore, from the analysis of the crack placed away from the contact patch (L = 7 mm) in Fig. 9b one can observe a comparable trend: the lower the maximum pressure, the higher crack driving force becomes with increasing the transversal force component. This is attributed to the crack opening fostered by greater transversal force component and reduced normal pressure. The competition between tensile, shear and compressive stress determines whether the crack opens or not. In contrast to the results for the crack location L = 5 mm, the increase of the crack driving forces due to transversal forces is observed also for contact patches with higher maximum pressure ($\geq$1300 MPa). This is because the crack is further away from the contact patch zone and thereby less affected by compressive stresses.

As the rails are exposed to not only dry but also wet conditions, the effect of different frictional properties at the crack faces is further analysed by finite element simulations. Fig. 10 shows the comparison of the calculated crack driving forces for the friction coefficient μ of 0, 0.25 and 0.50. As it can be seen in Fig. 10a, reduced friction can almost double the crack driving forces of the crack placed next to the contact patch (L = 5 mm) but only for higher maximum pressure (1500 – 1900 MPa). By contrast, given that the crack is far away from the contact patch zone (see Fig. 10b, L = 7 mm), altering the frictional properties at the crack faces has no effect on either the magnitude or the orientation of the crack driving force.

It should be noted in addition that the effect of moisture can also manifest in other ways like, for instance, exerting a pressure on the crack faces in the presence of a fluid filling the crack. This may affect the cracks just below (e.g. L = 0,1,3 mm), however not those away from the contact load (L = 5,7 mm). Besides, these effects have already been considered elsewhere: both numerical [3–5,7,12,20,37] and experimental [1,8,21,22,27,34] research have already shown that water or other fluid contamination promotes the growth of RCF cracks. In particular, the fluid pressure on the crack faces prevents the crack closure, leaving in addition the crack faces free from the friction forces. This in turn favours both mode I and mode II loading.

## 5. Summary and conclusion

The goal of this computational study was to benchmark the impact of the rail-wheel contact patch and its variations on the squat-like crack development. The propagation of a surface crack is assessed for the maximum pressure interval of 1000–2000 MPa. Gradually moving the crack away from the centre of the contact patch, it was found that only if the crack is on the boarder or outside

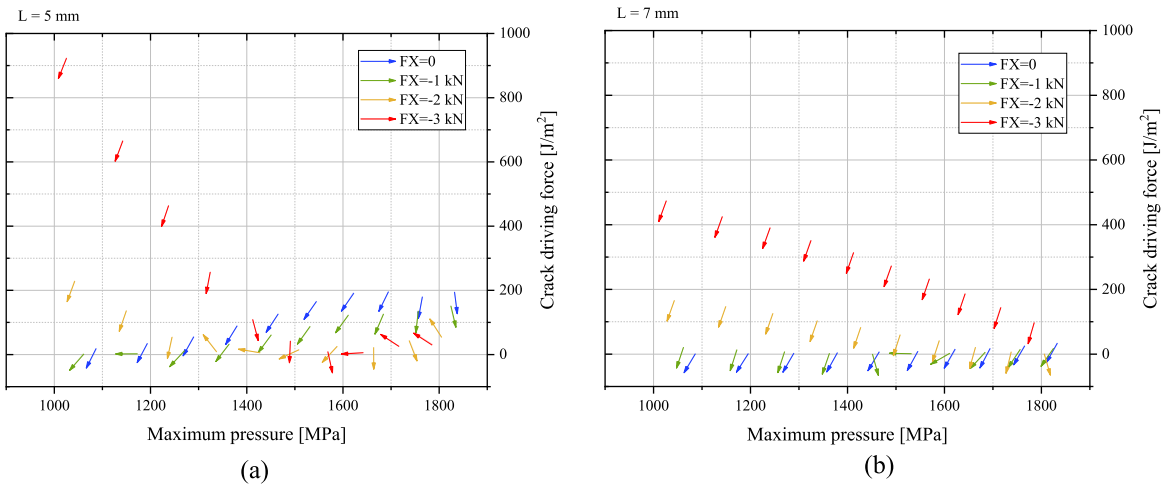


**Fig. 9.** Numerical study of the effect of transversal forces in a rail-wheel contact on the development of the crack driving force at the crack tip for the initial crack position L of (a) 5 mm and (b) 7 mm. The transversal force FX is varied between 0 and 3 kN.

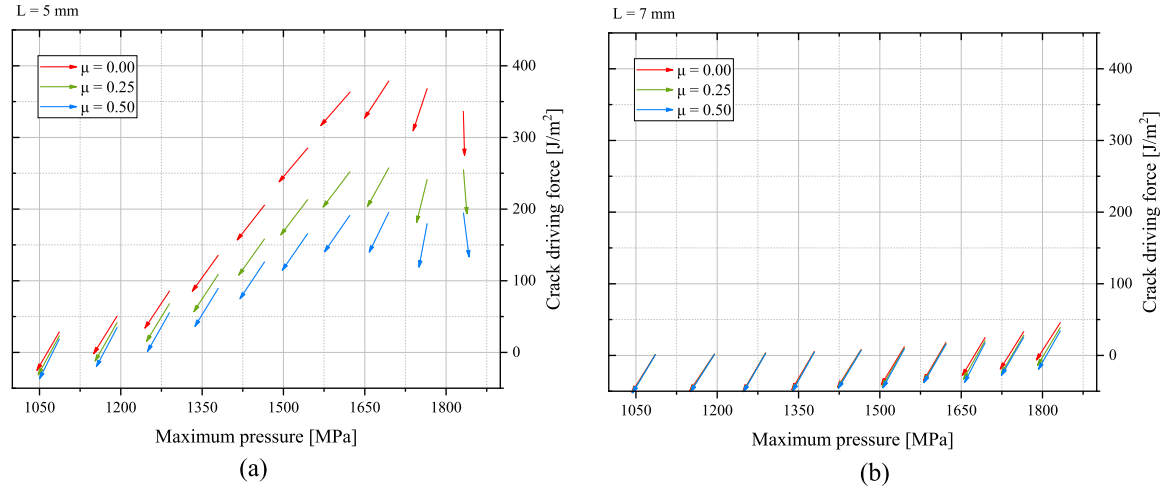


**Fig. 10.** Numerical study of the effect of the frictional properties at the crack faces on the development of the crack driving force at the crack tip for the initial crack position L of (a) 5 mm and (b) 7 mm. The friction coefficient μ is varied in the range of 0.0 – 0.50.

the contact patch zone, it can grow downward inside the rail profile. This provides a rational to squat-type cracks initiated from a head check-like surface defect near the running band at the gauge corner of the rail, which is often the preferred morphology of a squat [6,11,14,23].

The position of the crack alone, however, does not appear to be sufficient to initiate the crack growth. For the particular study cases analysed here, the numerical results showed that for the cracks nearby the contact patch, the presence of a transverse force can double the crack driving forces. Furthermore, it is found that the action of transversal forces is more dangerous for wheel-rail contact patches with lower maximum pressure. In other words, the interplay between compressive, shear and tensile stress determines the crack development. In addition, finite element analyses showed that wet conditions can also promote the crack growth insofar as the surface crack is outside but close enough to the contact patch zone.

These results suggest that lighter trains, such as passenger trains, might be even more dangerous for squat initiation than heavy freight trains. This is in accordance with statistical analysis [35], which reported that on the selected routes affected by squats, passenger trains made more than 88% of the rail traffic. Moreover, higher crack driving forces calculated for cracks having low friction coefficient at the crack faces explain the fact why squats are usually found on railways exposed to external influences while only rarely in tunnels. Having quantified different mechanical influences on the squat-like crack growth, the present study can foster the reproducibility of squats under controlled laboratory conditions, i.e. on a test rig.

*CRediT authorship contribution statement*

**Sandra Baltic:** Conceptualization, Methodology, Software, Writing – Original Draft, Writing – Review & Editing. **Werner Daves:** Supervision, Writing – Review & Editing, Project administration, Funding acquisition.

## Declaration of Competing Interest

The authors declare that they have no known competing financial interests or personal relationships that could have appeared to influence the work reported in this paper.

## Acknowledgements

The authors gratefully acknowledge the financial support under the scope of the COMET program within the K2 Center "Integrated Computational Material, Process and Product Engineering (IC-MPPE)" (Project No 886385). This program is supported by the Austrian Federal Ministries for Climate Action, Environment, Energy, Mobility, Innovation and Technology (BMK) and for Digital and Economic Affairs (BMDW), represented by the Austrian Research Promotion Agency (FFG), and the federal states of Styria, Upper Austria and Tyrol.

## References

[1] Al-Juboori A, Zhu H, Wexler D, Li H, Lu C, McCusker A, et al. Evolution of rail surface degradation in the tunnel: The role of water on squat growth under service conditions. Engng Fract Mech 2019;209:32–47. https://doi.org/10.1016/j.engfracmech.2019.01.018.
[2] ANSYS Documentation (2020): https://ansyshelp.ansys.com/, checked on 11/15/2021.
[3] Bogdański S. A rolling contact fatigue crack driven by squeeze fluid film. Fatigue Fract Engng Mater Struct 2002;25(11):1061–71. https://doi.org/10.1046/j.1460-2695.2000.00563.x.
[4] Bogdański S. Liquid–solid interaction at opening in rolling contact fatigue cracks. Wear 2005;258(7):1273–9. https://doi.org/10.1016/j.wear.2004.03.037.
[5] Bogdański S. Quasi-static and dynamic liquid solid interaction in 3D squat-type cracks. Wear 2014;314(1):20–7. https://doi.org/10.1016/j.wear.2013.11.023.
[6] Bogdański S, Brown MW. Modelling the three-dimensional behaviour of shallow rolling contact fatigue cracks in rails. Wear 2002;253(1):17–25. https://doi.org/10.1016/S0043-1648(02)00078-9.
[7] Bogdański S, Lewicki P. 3D model of liquid entrapment mechanism for rolling contact fatigue cracks in rails. Wear 2008;265(9):1356–62. https://doi.org/10.1016/j.wear.2008.03.014.
[8] Bogdański S, Lewicki P, Szymaniak M. Experimental and theoretical investigation of the phenomenon of filling the RCF crack with liquid. Wear 2005;258(7):1280–7. https://doi.org/10.1016/j.wear.2004.03.038.
[9] Bonniot T, Doquet V, Mai SH. Fatigue crack growth under non-proportional mixed-mode I + II. Role of compression while shearing. Int J Fatigue 2020;134:105513. https://doi.org/10.1016/j.ijfatigue.2020.105513.
[10] Clayton P. Tribological aspects of wheel-rail contact: a review of recent experimental research. Wear 1996;191(1):170–83. https://doi.org/10.1016/0043-1648(95)06651-9.
[11] Clayton P, Allery MBP. Metallurgical Aspects of Surface Damage Problems in Rails. Can Metall Q 1982;21(1):31–46. https://doi.org/10.1179/cmq.1982.21.1.31.
[12] Datsyshyn OP. Service life and fracture of solid bodies under the conditions of cyclic contact interaction. Mater Sci 2005;41(6):709. https://doi.org/10.1007/s11003-006-0037-1.
[13] Daves W, Kráčalík M, Scheriau S. Analysis of crack growth under rolling-sliding contact. Int J Fatigue 2019;121:63–72. https://doi.org/10.1016/j.ijfatigue.2018.12.006.
[14] Deroche RY, Bettembourg JP, Prasil B, Bertrand JP, Juckum C. Rolling Contact Fatigue Cracks on S.N.C.F Conventionnal Tracks. In: Kalker JJ, Cannon DF, Orringer O, editors. Rail Quality and Maintenance for Modern Railway Operation: International Conference on Rail Quality and Maintenance for Modern Railway Operation Delft. Dordrecht: Springer Netherlands; 1993. p. 435–48.
[15] Doquet V, Bertolino G. A material and environment-dependent criterion for the prediction of fatigue crack paths in metallic structures. Engng Fract Mech 2008;75(11):3399–412. https://doi.org/10.1016/j.engfracmech.2007.07.004.
[16] Eshelby JD. The force on an elastic singularity. Philos Trans R Soc Lond. Series A, Mathematical and Physical Sciences 1951;244(877):87–112. https://doi.org/10.1098/rsta.1951.0016.
[17] Eshelby JD. Energy relations and the energy-momentum tensor in continuum mechanics. Inelastic Behavior of Solids: The Energy Momentum Tensor in Continuum Mechanics; 1970. p. 77–115.
[18] Farjoo M, Daniel W, Bellette P, Meehan P. Field statistical and finite element analysis of rail squats. Engng Fract Mech 2013;109:117–29. https://doi.org/10.1016/j.engfracmech.2013.05.004.
[19] Farjoo M, Daniel W, Meehan PA. Modelling a squat form crack on a rail laid on an elastic foundation. Engng Fract Mech 2012;85:47–58. https://doi.org/10.1016/j.engfracmech.2012.02.004.
[20] Farjoo M, Pal S, Daniel W, Meehan PA. Stress intensity factors around a 3D squat form crack and prediction of crack growth direction considering water entrapment and elastic foundation. Engng Fract Mech 2012;94:37–55. https://doi.org/10.1016/j.engfracmech.2012.07.011.
[21] Fletcher, D. I.; Beynon, J. H. (1999): The influence of lubricant type on rolling contact fatigue of pearlitic rail steel. In D. Dowson, M. Priest, C. M. Taylor, P. Ehret, T.H.C. Childs, G. Dalmaz et al. (Eds.): Tribology Series : Lubrication at the Frontier, vol. 36: Elsevier, pp. 299–310. Available online at https://www.sciencedirect.com/science/article/pii/S0167892299800510.
[22] Fletcher DI, Hyde P, Kapoor A. Modelling and full-scale trials to investigate fluid pressurisation of rolling contact fatigue cracks. Wear 2008;265(9):1317–24. https://doi.org/10.1016/j.wear.2008.02.025.
[23] Grassie S. Squats and squat-type defects in rails: The understanding to date. Proceedings of the Institution of Mechanical Engineers, Part F: Journal of Rail and Rapid Transit 2011;226:235–42. https://doi.org/10.1177/0954409711422189.
[24] IN2TRACK Project Report - Research into enhanced tracks, switches and structures (2018): https://projects.shift2rail.org/s2r_ip3_n.aspx?p=IN2TRACK, checked on 4/12/2022.
[25] Jörg A, Stock R, Scheriau S, Brantner HP, Knoll B, Mach M, Daves W. The Squat Condition of Rail Materials - a Novel Approach to Squat Prevention. *Proceedings of the 10th International Conference on Contact Mechanics CM2015, Colorado Springs, USA*, p. 8. 2015.
[26] Kaewunruen S, Ishida M, Marich S. Dynamic Wheel-Rail Interaction Over Rail Squat Defects. Acoustics Australia 2015;43(1):97–107.
[27] Kaneta M, Matsuda K, Murakami K, Nishikawa H. A Possible Mechanism for Rail Dark Spot Defects. J Tribol 1998;120(2):304–9. https://doi.org/10.1115/1.2834426.

[28] Kerr, M.; Wilson, A.; Marich, S. (2008): The Epidemiology of Squats and Related Rail Defects. *Proceedings of CORE 2008 Conference on Railway Engineering: Rail-the-Core of Integrated Transport, Perth, 7-10 September 2008*, pp. 83-96.
[29] Kolednik O, Predan J, Fischer FD. Reprint of "Cracks in inhomogeneous materials: Comprehensive assessment using the configurational forces concept". Engng Fract Mech 2010;77(18):3611–24. https://doi.org/10.1016/j.engfracmech.2010.10.010.
[30] Kolednik O, Schöngrundner R, Fischer FD. A new view on J-integrals in elastic–plastic materials. Int J Fract 2014;187(1):77–107. https://doi.org/10.1007/s10704-013-9920-6.
[31] Kráčalík M, Daves W, Antretter T. Calculation of crack driving forces of surface cracks subjected to rolling/sliding contact. Engng Fract Mech 2016;152:10–25. https://doi.org/10.1016/j.engfracmech.2015.12.003.
[32] Kráčalík M, Daves W, Scheriau S. Finite Element Investigation of the Load Influence on Shear Crack Direction and Growth in Wheel-Rail Contact. In: Iványi P, Topping BHV, editors. Proceedings of the Ninth International Conference on Engineering Computational Technology; 2014. https://doi.org/10.4203/ccp.105.22.
[33] Li Z, Zhao X, Dollevoet R, Molodova M. Differential wear and plastic deformation as causes of squat at track local stiffness change combined with other track short defects. Veh Syst Dyn 2008;46(sup1):237–46. https://doi.org/10.1080/00423110801935855.
[34] Maya-Johnson S, Felipe Santa J, Toro A. Dry and lubricated wear of rail steel under rolling contact fatigue - Wear mechanisms and crack growth. Wear 2017;380–381:240–50. https://doi.org/10.1016/j.wear.2017.03.025.
[35] Muhamedsalih Y, Hawksbee S, Tucker G, Stow J, Burstow M. Squats on the Great Britain rail network: Possible root causes and research recommendations. Int J Fatigue 2021;149:106267. https://doi.org/10.1016/j.ijfatigue.2021.106267.
[36] Norm EN 17397-1. Bahnanwendungen - Schienenfehler - Teil 1: Handhabung von Schienenfehlern: 2021.
[37] Olzak M, Stupnicki J, Wojcik R. Investigation of crack propagation during contact by a finite element method. Wear 1991;146(2):229–40. https://doi.org/10.1016/0043-1648(91)90065-3.
[38] Rasmussen CJ, Fæster S, Dhar S, Quaade JV, Bini M, Danielsen HK. Surface crack formation on rails at grinding induced martensite white etching layers. Wear 2017;384–385:8–14. https://doi.org/10.1016/j.wear.2017.04.014.
[39] Rice JR. A Path Independent Integral and the Approximate Analysis of Strain Concentration by Notches and Cracks. Appliedmechanics 1968;35(2):379–86. https://doi.org/10.1115/1.3601206.
[40] Schnalzger G, Maierhofer J, Daves W, Pippan R, Hohenwarter A. Fatigue crack growth of deformed pearlitic rail steels under multiaxial loading. Procedia Struct Integrity 2022;39:313–26. https://doi.org/10.1016/j.prostr.2022.03.101.
[41] Simha NK, Fischer FD, Shan GX, Chen CR, Kolednik O. J-integral and crack driving force in elastic–plastic materials. J Mech Phys Solids 2008;56(9):2876–95. https://doi.org/10.1016/j.jmps.2008.04.003.
[42] Simha NK, Fischer FD, Kolednik O, Chen CR. Inhomogeneity effects on the crack driving force in elastic and elastic–plastic materials. J Mech Phys Solids 2003;51(1):209–40. https://doi.org/10.1016/S0022-5096(02)00025-X.
[43] Simon S, Saulot A, Dayot C, Quost X, Berthier Y. Tribological characterization of rail squat defects. Wear 2013;297(1):926–42. https://doi.org/10.1016/j.wear.2012.11.011.
[44] Steenbergen M, Dollevoet R. On the mechanism of squat formation on train rails – Part I: Origination. Int J Fatigue 2013;47:361–72. https://doi.org/10.1016/j.ijfatigue.2012.04.023.
[45] Steenbergen M, Dollevoet R. On the mechanism of squat formation on train rails – Part II: Growth. Int J Fatigue 2013;47:373–81. https://doi.org/10.1016/j.ijfatigue.2012.04.019.
[46] Code UIC. 712: Rail defects. 4th ed.: Paris: International Union of Railways; 2002.
[47] Wasén J, Heier E. Fatigue crack growth thresholds—the influence of Young's modulus and fracture surface roughness. Int J Fatigue 1998;20(10):737–42. https://doi.org/10.1016/S0142-1123(98)00034-6.
[48] Zerbst U, Vormwald M, Pippan R, Gänser H-P, Sarrazin-Baudoux C, Madia M. About the fatigue crack propagation threshold of metals as a design criterion – A review. Engng Fract Mech 2016;153:190–243. https://doi.org/10.1016/j.engfracmech.2015.12.002.